QCD corrections to $t\bar{b}H^-$ associated production in e^+e^- annihilation

Bernd A. Kniehl*
CERN, Theoretical Physics Division, 1211 Geneva 23, Switzerland

Fantina Madricardo and Matthias Steinhauser
II. Institut für Theoretische Physik, Universität Hamburg, Luruper Chaussee 149, 22761 Hamburg, Germany
(Received 28 May 2002; published 30 September 2002)

We calculate the QCD corrections to the cross section of $e^+e^-\to t\bar{b}H^-$ and its charge-conjugate counterpart within the minimal supersymmetric extension of the standard model. This process is particularly important if $m_t<m_H+m_b$ and $\sqrt{s}<2m_H$, so that $t\to bH^+$ and $e^+e^-\to H^+H^-$ are not allowed kinematically. Large logarithmic corrections that arise in the on-mass-shell scheme of quark mass renormalization, especially from the $t\bar{b}H^-$ Yukawa coupling for large values of $\tan\beta$, are resummed by adopting the modified minimal-subtraction scheme, so that the convergence behavior of the perturbative expansion is improved. The inclusion of the QCD corrections leads to a significant reduction of the theoretical uncertainties due to scheme and scale dependences.

DOI: 10.1103/PhysRevD.66.054016 PACS number(s): 12.38.Bx, 12.60.Jv, 13.10.+q

I. INTRODUCTION

One of the prime objectives of a future e^+e^- linear collider (LC) will be the detailed study of spin-zero particles which remain in the physical spectrum after the elementary-particle masses have been generated through the Higgs mechanism of electroweak symmetry breaking. Should the world be supersymmetric, then the Higgs sector is more complicated than in the standard model (SM), which predicts just one neutral CP-even Higgs boson H. The Higgs sector of the minimal supersymmetric extension of the SM (MSSM) consists of a two-Higgs-doublet model (2HDM) and accommodates five physical Higgs bosons: the neutral CP-even h^0 and H^0 bosons, the neutral CP-odd A^0 boson, and the charged $H^\pm$-boson pair. The 2HDM has six free parameters, which are usually taken to be the masses m_{h^0}, m_{H^0}, m_{A^0}, and $m_{H^\pm}$, the ratio $\tan\beta=v_2/v_1$ of the vacuum expectation values of the two Higgs doublets, and the weak mixing angle α that relates the weak and mass eigenstates of h^0 and H^0. At the tree level, the MSSM Higgs sector has just two free parameters, which are usually taken to be the m_{A^0} and $\tan\beta$.

The discovery of the $H^\pm$ bosons would prove the SM wrong and, at the same time, give strong support to the 2HDM and the MSSM. If the $H^\pm$ bosons have mass $m_H<m_t-m_b$, they will be mainly produced through the $t\to bH^+$ decays of top quarks, which are copiously generated singly or in pairs at an e^+e^- LC [1]. On the other hand, if there is sufficient center-of-mass (c.m.) energy available, $\sqrt{s}>2m_H$, then charged-Higgs-boson pair production, $e^+e^-\to H^+H^-$, will be the dominant production mechanism [1]. Otherwise, if $m_H>\max(m_t-m_b,\sqrt{s}/2)$, the $H^\pm$ bosons can still be produced singly. There are various mechanisms of single-charged-Higgs-boson production [2]. The most important of them are $e^+e^-\to W^+H^-$, which proceeds through quantum loops involving SM [3,4] and possibly supersymmetric [4] particles, $e^+e^-\to\tau^+\nu_\tau H^-$ [2,5], and $e^+e^-\to t\bar{b}H^-$ [2,6].

In the following, we are concerned with the latter process. The cross section of this process exhibits a strong dependence on $\tan\beta$, so that its measurement provides an opportunity to directly determine this crucial parameter. At the tree level, this reaction proceeds through the Feynman diagrams depicted in Fig. 1. It is kinematically allowed if $\sqrt{s}>m_t+m_b+m_H$. Hence, we are most interested in a situation where $m_t+m_b<\sqrt{s}/2<m_H<\sqrt{s}-m_t-m_b$. For $\sqrt{s}=500$ GeV (800 GeV), this implies that $250\lesssim m_H\lesssim 320$ GeV ($400\lesssim m_H\lesssim 620$ GeV). In such a situation, none of the virtual particles appearing in Fig. 1 can be resonating. We note in passing that the absence of resonances is also guaranteed if $m_t-m_b<m_H<m_t+m_b$ [6]. However, this process is then of minor interest because we always have $\sqrt{s}>2m_H$, so that $e^+e^-\to H^+H^-$ will take place. In the presence of a resonance, the cross section approximately factorizes. Specifically, we have $\sigma(e^+e^-\to t\bar{b}H^-)\approx\sigma(e^+e^-\to t\bar{t})B(\bar{t}\to\bar{b}H^-)$ when the virtual $\bar{t}$ quark gets on its mass shell, while we have $\sigma(e^+e^-\to t\bar{b}H^-)\approx\sigma(e^+e^-$

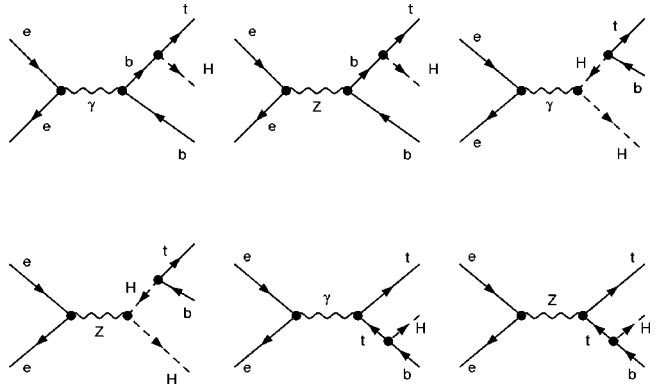

FIG. 1. Tree-level Feynman diagrams pertinent to the process $e^+e^-\to t\bar{b}H^-$.

*Permanent address: II. Institut für Theoretische Physik, Universität Hamburg, Luruper Chaussee 149, 22761 Hamburg, Germany.

$\to H^+H^-)B(H^+\to t\bar{b})$ when the virtual H^+ boson gets on its mass shell.

The purpose of this paper is to investigate the dominant quantum corrections to the cross section of $e^+e^-\to t\bar{b}H^-$, which arise from quantum chromodynamics (QCD). The relevant Feynman diagrams emerge by attaching one gluon line in all possible ways to each of the diagrams shown in Fig. 1. This leads to $2\to3$ diagrams with one closed loop (see Fig. 2), which yield the virtual corrections, and to $2\to4$ diagrams of the tree-level type (see Fig. 3), which give rise to the real corrections. The loop diagrams involve two, three, or four virtual particles.

While the QCD corrections to the cross sections of the related processes $e^+e^-\to q\bar{q}\Phi$, where $q=t,b$ and $\Phi=H$ [7,8] or $\Phi=h^0,H^0,A^0$ [9], are available in the literature, the corresponding analysis for $e^+e^-\to t\bar{b}H^-$ has been lacking so far. The present paper fills this gap.

The cross section of the SM process $e^+e^-\to q\bar{q}H$ via a virtual photon and its QCD corrections can be recovered from our results as a special case, involving only a subclass of the Feynman diagrams shown in Figs. 1–3. As a by-product of our analysis, we confirm the numerical results for this cross section obtained in Refs. [7,8]. We also perform the complete calculation for this process, which involves Feynman diagrams where the H boson is radiated off a virtual Z-boson line, and find good agreement with Ref. [7].

This paper is organized as follows. In Sec. II, we list a compact Born formula for the cross section of $e^+e^-\to t\bar{b}H^-$ and give details of our analytical calculation of its virtual and real QCD corrections. Lengthy expressions are relegated to Appendices A and B, where the Born form factors and the parametrization of the four-particle phase space, respectively, may be found. In Sec. III, we present our numerical results. In Sec. IV, we conclude with a summary of our analysis.

II. ANALYTIC RESULTS

In this section, we list a compact Born formula for the cross section of $e^+e^-\to t\bar{b}H^-$ and give details of our analytical calculation of its virtual and real QCD corrections. By charge-conjugation invariance, the results for $e^+e^-\to\bar{t}bH^+$ are the same.

A. Born cross section

We start by defining the kinematics. We call the four-momenta of the incoming electron and positron k_1 and k_2 and those of the outgoing t quark, $\bar{b}$ quark, and H^- boson p_1, p_2, and p_3, respectively. We neglect the electron mass, but retain the b-quark mass, so that the on-mass-shell (OS) conditions read $k_1^2=k_2^2=0$, $p_1^2=m_t^2$, $p_2^2=m_b^2$, and $p_3^2=m_H^2$. The virtual photon and Z boson have four-momentum $p=k_1+k_2=p_1+p_2+p_3$, and we define $s=p^2$. It is convenient to introduce the dimensionless Lorentz scalars $a_i=p_i^2/s$, $x_i=2p\cdot p_i/s$, and $y_i=\sqrt{x_i^2-4a_i}$ $(i=1,2,3)$. In the c.m. frame, $x_i=2p_i^0/\sqrt{s}$ and $y_i=2|\boldsymbol{p}_i|/\sqrt{s}$ carry the meaning of scaled energies and absolute three-momenta, respectively. By four-momentum conservation, we have $x_1+x_2+x_3=2$.

The differential Born cross section may be evaluated as

$$d\sigma_{\rm Born}=\frac{1}{2s}\frac{1}{4}|\mathcal{T}_{\rm Born}|^2 d{\rm PS}_3(p;p_1,p_2,p_3), \tag{2.1}$$

where the first and second factors on the right-hand side stem from the flux and the average over the lepton spins, respectively, $\mathcal{T}_{\rm Born}$ is the transition-matrix element corresponding to the Feynman diagrams of Fig. 1, and the summation over the lepton and quark spins is implied. We assume that the incoming leptons are unpolarized. Here and in the following, we define the Lorentz-invariant n-particle phase-space measure as

$$d{\rm PS}_n(p;p_1,\ldots,p_n)=(2\pi)^4\delta^{(4)}\left(p-\sum_{i=1}^n p_i\right)\prod_{i=1}^n\frac{d^3p_i}{(2\pi)^3 2p_i^0}. \tag{2.2}$$

We now discuss the parametrization of the three-particle phase space. We wish to express the Born cross section differential with respect to the scaled energies of the final-state quarks, x_1 and x_2. For convenience, we work in the c.m. frame, define the z axis of the coordinate system to point along $\boldsymbol{k}_1=-\boldsymbol{k}_2$, and fix the x axis in an arbitrary way. We then have

$$d{\rm PS}_3(p;p_1,p_2,p_3)=\frac{4}{(4\pi)^5}dp_1^0\,d\cos\theta_1\,d\phi_1\,dp_2^0\,d\phi_2, \tag{2.3}$$

where θ_1 and ϕ_1 are the polar and azimuthal angles of $\boldsymbol{p}_1$, respectively, and ϕ_2 is the azimuthal angle of $\boldsymbol{p}_2$ with respect to the axis pointing along $\boldsymbol{p}_1$ measured from the plane spanned by $\boldsymbol{k}_1$ and $\boldsymbol{p}_1$. Because of the azimuthal symmetry of the problem at hand, the integration over ϕ_1 is trivial, and we may take $\boldsymbol{p}_1$ to lie in the x-z plane. If we now rotate the coordinate system in such a way that $\boldsymbol{p}_1$ points along the z axis and $\boldsymbol{p}_2$ lies in the x-z plane, then $\theta=\theta_1$ and $\phi=\pi-\phi_2$ define the direction of $\boldsymbol{k}_1$. We thus have

$$d{\rm PS}_3(p;p_1,p_2,p_3)=\frac{s}{2(4\pi)^4}dx_1\,dx_2\,d\cos\theta\,d\phi. \tag{2.4}$$

Next, we observe that $|\mathcal{T}_{\rm Born}|^2$ can be written as a contraction of two rank-two tensors, a leptonic one involving k_1 and k_2 and a quarkonic one involving p_1, p_2, and p_3. The leptonic one has the form

$$L^{\mu\nu}={\rm tr}\not{k}_1\gamma^\nu(v_e'-a_e'\gamma_5)\not{k}_2\gamma^\mu(v_e-a_e\gamma_5), \tag{2.5}$$

where v_e, v_e', a_e, and a_e' are generic vector and axial-vector couplings of the electron to the photon or Z boson. Performing the integrations over $\cos\theta$ and ϕ, we obtain

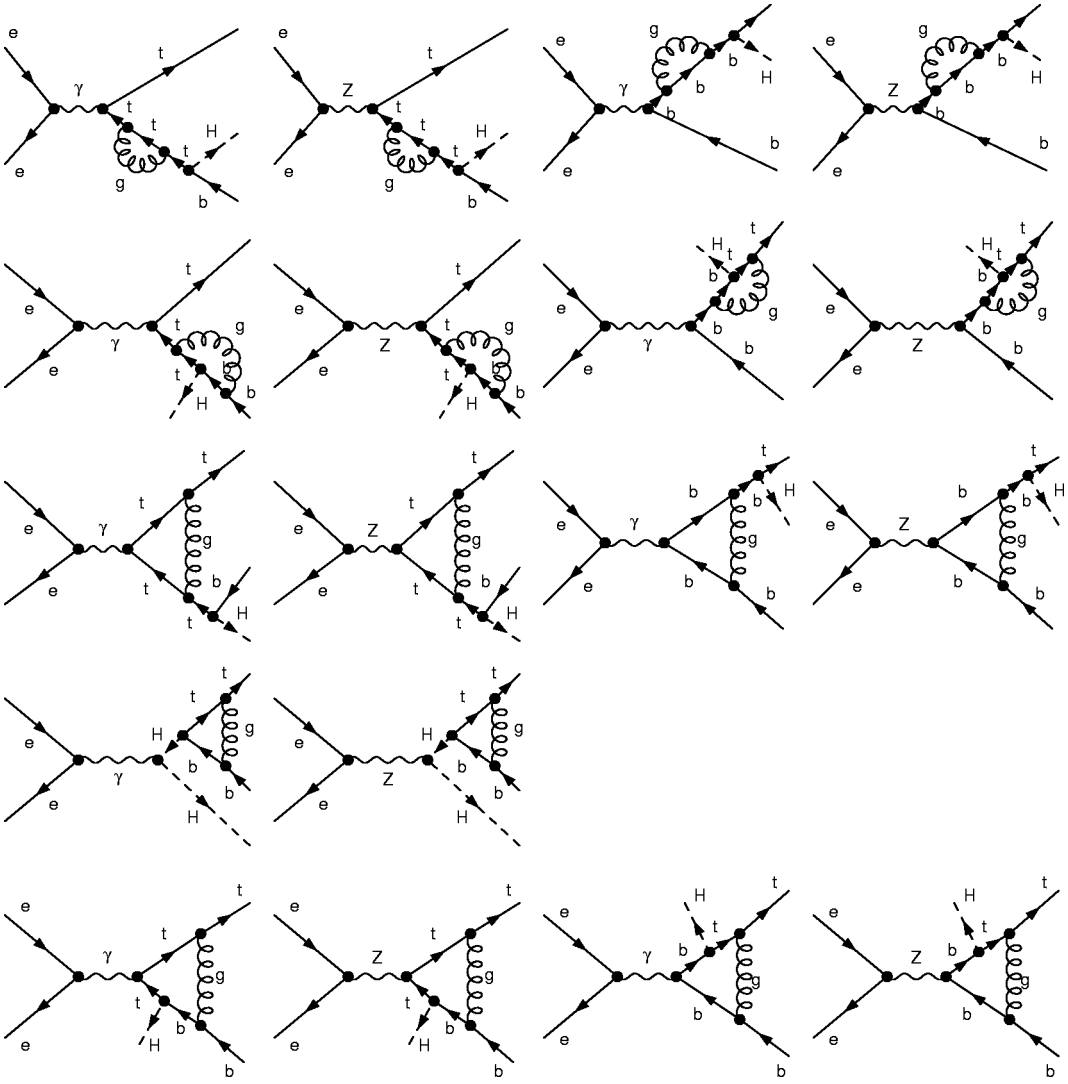

FIG. 2. One-loop Feynman diagrams pertinent to the process $e^+e^-\to t\bar{b}H^-$. They are classified according to the number of propagators in the loops.

$$\int \frac{d\Omega}{4\pi} L^{\mu\nu} = \frac{4}{3}(v_e v_e' + a_e a_e')(p^\mu p^\nu - s g^{\mu\nu}). \quad (2.6)$$

The fact that Eq. (2.6) just depends on p dramatically simplifies the remaining phase-space integrations, since scalar products of the type $k_i \cdot p_j$ are precluded. The residual scalar products are $p_i \cdot p_j = (s/2)(z_k - a_i - a_j)$, where $z_k = 1 + a_k - x_k$, with $i,j,k = 1,2,3$ and $i \neq j \neq k \neq i$.

We thus find the doubly-differential Born cross section to be

$$\frac{d\sigma_{\rm Born}}{dx_1\,dx_2} = \frac{G_F^3 m_Z^4}{32\pi^3\sqrt{2}}[\mathcal{Q}_e^2 f_{\gamma\gamma}(x_1,x_2) + \mathcal{Q}_e \mathcal{V}_e f_{\gamma Z}(x_1,x_2) + (\mathcal{V}_e^2 + \mathcal{A}_e^2) f_{ZZ}(x_1,x_2)], \quad (2.7)$$

where G_F is Fermi's constant,

$$\mathcal{Q}_e = -2 c_w s_w Q_e, \quad \mathcal{V}_e = \frac{I_e - 2 s_w^2 Q_e}{1 - m_Z^2/s}, \quad \mathcal{A}_e = \frac{I_e}{1 - m_Z^2/s}, \quad (2.8)$$

and $f_{\gamma\gamma}(x_1,x_2)$, $f_{\gamma Z}(x_1,x_2)$, and $f_{ZZ}(x_1,x_2)$ are form factors listed in Appendix A. Here, $s_w^2 = 1 - c_w^2 = 1 - m_W^2/m_Z^2$ is the sine square of the weak mixing angle, m_W and m_Z are the masses of the W and Z bosons, respectively, $Q_e = -1$ is the electric charge of the electron, and $I_e = -1/2$ is the third component of weak isospin of its left-handed component.

The boundaries of integration are

$$2\sqrt{a_1} < x_1 < 1 + a_1 - (\sqrt{a_2} + \sqrt{a_3})^2, \quad x_2^- < x_2 < x_2^+, \quad (2.9)$$

with

$$x_2^\pm = \frac{1}{2z_1}[(2 - x_1)(z_1 + a_2 - a_3) \pm y_1 \sqrt{\lambda(z_1,a_2,a_3)}], \quad (2.10)$$

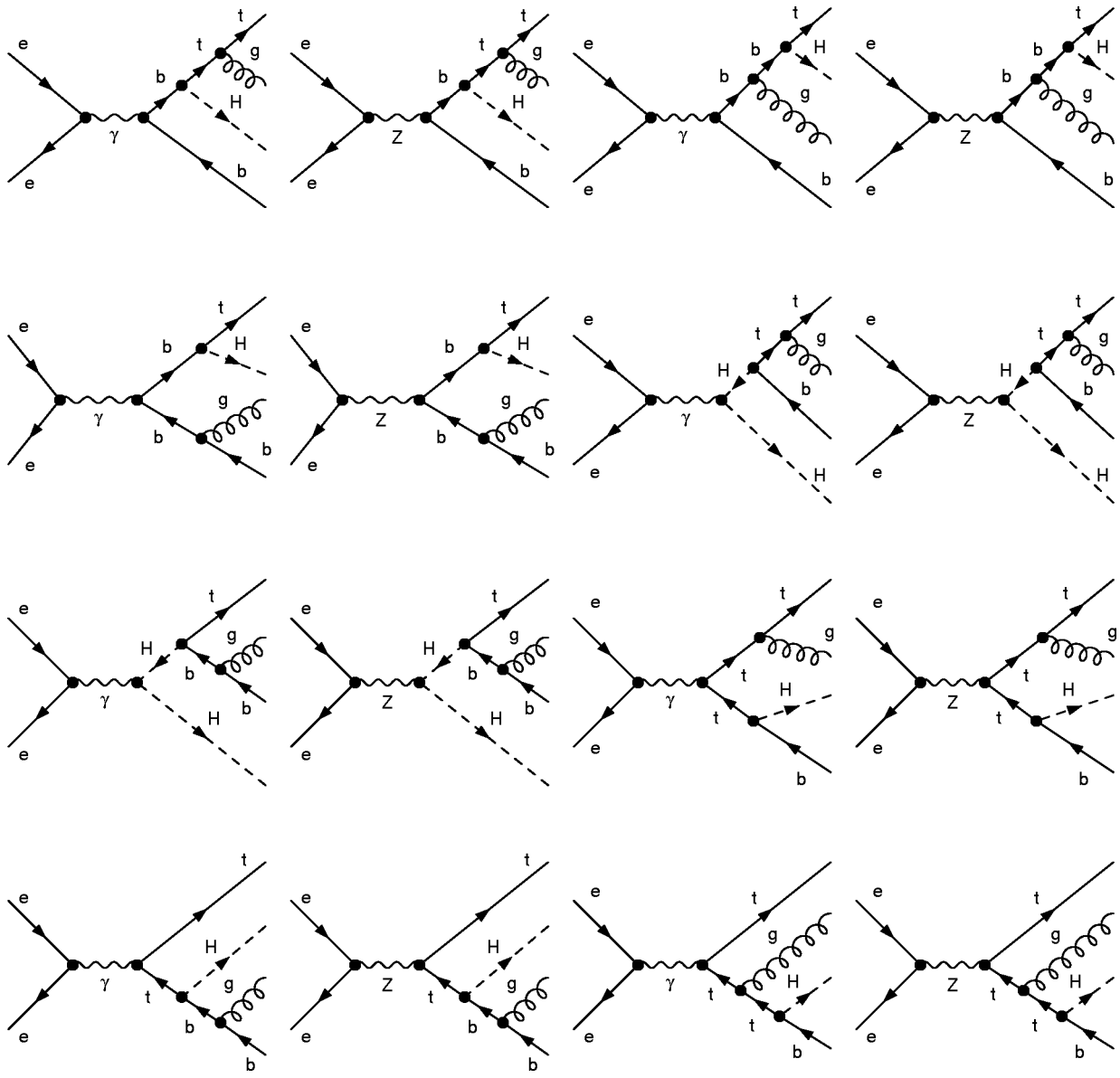

FIG. 3. Tree-level Feynman diagrams pertinent to the process $e^+e^-\to t\bar{b}gH^-$.

where $\lambda(x,y,z)=x^2+y^2+z^2-2(xy+yz+zx)$ is Källén's function. We perform the integrations over x_1 and x_2 numerically with the aid of the multi-dimensional Monte Carlo integration routine VEGAS [10].

B. Virtual corrections

We now turn to the virtual QCD corrections, which arise from the one-loop Feynman diagrams shown in Fig. 2. Specifically, they include *t*- and *b*-quark self-energy corrections; $t\bar{t}\gamma$, $t\bar{t}Z$, $b\bar{b}\gamma$, $b\bar{b}Z$, and $t\bar{b}H^-$ vertex corrections; and $t\bar{b}\gamma H^-$ and $t\bar{b}ZH^-$ box corrections. These corrections suffer both from infrared (IR) and ultraviolet (UV) divergences. We regularize the former by endowing the gluon with an infinitesimal mass, m_g. In our case, this does not spoil gauge invariance, since the non-Abelian nature of QCD does not yet emerge at next-to-leading order (NLO). This leads to terms logarithmic in m_g, which combine with similar terms arising from soft-gluon emission, to be discussed below, to give a m_g-independent result. We establish this cancellation analytically.

UV divergences only occur in the self-energy and vertex corrections. We extract them using dimensional regularization, with $D=4-2\epsilon$ space-time dimensions and 't Hooft mass scale μ. They are removed by renormalization. Specifically, we need to renormalize the quark masses and wave functions appearing in $\mathcal{T}_{\rm Born}$. Notice that the quark masses enter not only through the quark propagators, but also through the $t\bar{b}H^-$ Yukawa coupling. To this end, we substitute $m_q\to m_q^0=m_q+\delta m_q$ and $\psi_q\to\psi_q^0=\psi_q\sqrt{1+\delta Z_2^q}$ ($q=t,b$), where bare quantities are denoted by the superscript 0. In the OS scheme, the renormalization constants read

$$\frac{\delta m_q}{m_q} = -\frac{\alpha_s}{4\pi} C_F \left[3\Delta + 3\ln\frac{\mu^2}{m_q^2} + 4 + \mathcal{O}(\epsilon) \right], \tag{2.11}$$

$$\delta Z_2^q = -\frac{\alpha_s}{4\pi} C_F \left[\Delta + \ln\frac{\mu^2}{m_q^2} + 2\ln\frac{m_g^2}{m_q^2} + 4 + \mathcal{O}(\epsilon) \right], \tag{2.12}$$

with $C_F = (N_c^2 - 1)/(2N_c) = 4/3$ for $N_c = 3$ quark colors and

$$\Delta = \frac{1}{\epsilon} - \gamma_E + \ln(4\pi), \tag{2.13}$$

where γ_E is the Euler-Mascheroni constant. Notice that Z_2^q is also IR divergent. The expression for $\delta m_q/m_q$ in the modified minimal-subtraction ($\overline{\text{MS}}$) scheme [11] emerges from Eq. (2.11) by retaining only the first term contained within the square brackets.

The virtual QCD corrections may be evaluated as

$$d\sigma_{\text{virt}} = d\sigma_{\text{Born}} \delta_{\text{virt}}(m_g), \tag{2.14}$$

with

$$\delta_{\text{virt}}(m_g) = \frac{2}{|\mathcal{T}_{\text{Born}}|^2} \text{Re}\left\{ \mathcal{T}_{\text{Born}}^* \left[\sum_{q=t,b} \left(\delta m_q \frac{\partial}{\partial m_q} + \frac{1}{2}\delta Z_2^q \right) \times \mathcal{T}_{\text{Born}} + \mathcal{T}_{\text{loop}} \right] \right\}, \tag{2.15}$$

where $\mathcal{T}_{\text{loop}}$ is the transition-matrix element corresponding to the Feynman diagrams of Fig. 2. Notice that the quark masses that appear in the squares of the quark spinors and in the boundaries of the phase-space integration correspond to renormalized ones from the outset. As mentioned above, $\delta_{\text{virt}}(m_g)$ is UV finite, but IR divergent. Notice that Eq. (2.6), which refers to the physical case $D = 4$, can still be used at the one-loop level, since the quarkonic tensor is by itself UV finite upon renormalization.

We generate $\mathcal{T}_{\text{loop}}$ and reduce it to standard one-loop scalar integrals in two independent ways: one is based on the combination of the program packages FEYNARTS [12] and FORMCALC [13] and the other one on custom-made routines written in the program language FORM [14]. We then evaluate the standard one-loop scalar integrals, the IR-divergent ones analytically using the results of Ref. [15] and the IR-finite ones numerically with the help of the program package LOOPTOOLS [13]. Our analytic result for $\delta_{\text{virt}}(m_g)$ is too lengthy to be presented here.

C. Real corrections

We now proceed to the real QCD corrections, which arise from the $2 \to 4$ tree-level Feynman diagrams shown in Fig. 3. We denote the gluon four-momentum by q. As mentioned above, the emission of soft gluons generates IR divergences. For consistency with the evaluation of the virtual QCD corrections, the latter must also be regularized by the gluon mass m_g. It is convenient to work in the c.m. frame and to introduce an unphysical gluon-energy cutoff, E_{cut}, with $m_g \ll E_{\text{cut}} \ll E_{\text{max}}$, where E_{max} is the maximum gluon energy allowed by kinematics, so as to separate the gluon phase space into soft and hard regions, defined by $m_g < q^0 < E_{\text{cut}}$ and $E_{\text{cut}} < q^0 < E_{\text{max}}$, respectively. This has two technical advantages, since soft gluons with infinitesimal mass m_g do not affect the kinematics of the underlying process, while hard gluons with zero mass do not produce IR divergences. On the one hand, the soft-gluon bremsstrahlung may be treated analytically in the eikonal approximation, which is independent of the underlying process and results in a multiplicative correction to the Born result. On the other hand, m_g may be safely neglected in the treatment of the hard-gluon bremsstrahlung, which facilitates the phase-space integration. In turn, the soft- and hard-gluon contributions both depend on E_{cut}, while their combined contribution is, of course, independent of E_{cut}, which we checked numerically. As mentioned above, the m_g dependence of the soft-gluon contribution analytically cancels against the one of the virtual QCD corrections.

The soft-gluon contribution is given by

$$d\sigma_{\text{soft}} = d\sigma_{\text{Born}} \delta_{\text{soft}}(m_g, E_{\text{cut}}), \tag{2.16}$$

with

$$\delta_{\text{soft}}(m_g, E_{\text{cut}}) = -\frac{\alpha_s C_F}{(2\pi)^2} \int_{|\boldsymbol{q}| < E_{\text{cut}}} \frac{d^3q}{q^0} \left(\frac{p_1}{p_1 \cdot q} - \frac{p_2}{p_2 \cdot q} \right)^2, \tag{2.17}$$

where $q^0 = \sqrt{\boldsymbol{q}^2 + m_g^2}$ is the gluon energy. The integration in Eq. (2.17) can be performed analytically as described in Ref. [16], the result being

$$\delta_{\text{soft}}(m_g, E_{\text{cut}}) = \frac{\alpha_s}{\pi} C_F \left\{ \left(\frac{\alpha}{2} \frac{z_3 - a_1 - a_2}{\alpha^2 a_1 - a_2} \ln\frac{\alpha^2 a_1}{a_2} - 1 \right) \ln\frac{4E_{\text{cut}}^2}{m_g^2} + \alpha \frac{z_3 - a_1 - a_2}{\alpha^2 a_1 - a_2} \left[\text{Li}_2\left(1 - \alpha \frac{x_1 + y_1}{v} \right) + \text{Li}_2\left(1 - \alpha \frac{x_1 - y_1}{v} \right) - \text{Li}_2\left(1 - \frac{x_2 + y_2}{v} \right) - \text{Li}_2\left(1 - \frac{x_2 - y_2}{v} \right) + \frac{1}{4}\left(\ln^2\frac{x_1 - y_1}{x_1 + y_1} - \ln^2\frac{x_2 - y_2}{x_2 + y_2} \right) \right] - \frac{1}{2}\left(\frac{x_1}{y_1} \ln\frac{x_1 - y_1}{x_1 + y_1} + \frac{x_2}{y_2} \ln\frac{x_2 - y_2}{x_2 + y_2} \right) \right\}, \tag{2.18}$$

where $\mathrm{Li}_2(x)=-\int_0^x dy\,\ln(1-y)/y$ is the Spence function,

$$\alpha=\frac{1}{2a_1}[z_3-a_1-a_2+\sqrt{\lambda(z_3,a_1,a_2)}],$$

$$v=2\frac{\alpha^2 a_1-a_2}{\alpha x_1-x_2}. \tag{2.19}$$

Notice that Eq. (2.18) is invariant under the interchange of the indices 1 and 2.

The hard-gluon contribution may be evaluated by integrating

$$d\sigma_{\mathrm{hard}}(E_{\mathrm{cut}})=\frac{1}{2s}\frac{1}{4}|\mathcal{T}_{\mathrm{real}}|^2\theta(q^0-E_{\mathrm{cut}}) \times d\mathrm{PS}_4(p;p_1,p_2,p_3,q), \tag{2.20}$$

where $\mathcal{T}_{\mathrm{real}}$ is the transition-matrix element corresponding to the Feynman diagrams of Fig. 3, over the full four-particle phase space, imposing the condition $q^0>E_{\mathrm{cut}}$. We use the parametrization of the four-particle phase space presented in Appendix B. It involves five nontrivial integrations, which we perform numerically using the Monte Carlo routine VEGAS [10]. Our formula for $|\mathcal{T}_{\mathrm{real}}|^2$ is too lengthy to be listed here.

We performed several checks for our implementation of the four-particle phase-space integration. We numerically verified the analytical formula for the total cross section of $e^+e^-\to q\bar{q}g^*\to q\bar{q}Q\bar{Q}$, where q and Q represent massless and massive quarks, respectively, and g^* denotes a virtual gluon, given in Eq. (2) of Ref. [17]. In this case, IR singularities do not appear in intermediate steps, so that no separation into soft-gluon and hard-gluon contributions is required. We also found excellent agreement with a numerical result for a similar process involving four different quark masses obtained using the democratic multi-particle phase-space generator RAMBO [18].

Our final result for the QCD-corrected differential cross section reads

$$d\sigma_{\mathrm{QCD}}=d\sigma_{\mathrm{Born}}[1+\delta_{\mathrm{virt}}(m_g)+\delta_{\mathrm{soft}}(m_g,E_{\mathrm{cut}})] + d\sigma_{\mathrm{hard}}(E_{\mathrm{cut}}), \tag{2.21}$$

where $d\sigma_{\mathrm{Born}}$, $\delta_{\mathrm{virt}}(m_g)$, $\delta_{\mathrm{soft}}(m_g,E_{\mathrm{cut}})$, and $d\sigma_{\mathrm{hard}}(E_{\mathrm{cut}})$ are defined in Eqs. (2.1), (2.15), (2.17), and (2.20), respectively. It is manifestly independent of m_g and insensitive to the choice of E_{cut}, as long as $m_g\ll E_{\mathrm{cut}}\ll E_{\mathrm{max}}$, as we verified numerically. We also checked that the QCD-corrected total cross section is finite in the limit $m_b\to 0$, in compliance with the Kinoshita-Lee-Nauenberg theorem [19].

The QCD-corrected cross section of the SM process $e^+e^-\to q\bar{q}H$ via a virtual photon can be obtained from our results as a special case, involving only a subclass of the Feynman diagrams shown in Figs. 1–3. As a by-product of our analysis, we confirmed the numerical results for this cross section obtained in Refs. [7,8]. We also performed the complete calculation for this process, which involves Feynman diagrams where the H boson is radiated off a virtual Z-boson line, and found good agreement with Ref. [7]. In turn, this provides a nontrivial check for all parts of our analysis.

III. NUMERICAL RESULTS

We are now in a position to present our numerical results. We first specify our input parameters. We use $m_W=80.419$ GeV, $m_Z=91.1882$ GeV, $m_t=174.3$ GeV, $m_b=4.6$ GeV, $G_F=1.16639\times10^{-5}$ GeV^{-2} [20], and the present world average $\alpha_s^{(5)}(m_Z)=0.1180$ [21]. We consistently evaluate $\alpha_s^{(n_f)}(\mu)$ and $\overline{m}_q^{(n_f)}(\mu)$ to lowest order (LO) in the $\overline{\mathrm{MS}}$ scheme with $n_f=6$ active quark flavors performing the matching with $n_f=5$ QCD at scale m_t. For the reader's convenience, we collect the relevant formulas here [22]:

$$\frac{1}{\alpha_s^{(5)}(\mu)}=\frac{1}{\alpha_s^{(5)}(m_Z)}+\frac{\beta_0^{(5)}}{\pi}\ln\frac{\mu^2}{m_Z^2}, \tag{3.1}$$

$$\frac{1}{\alpha_s^{(6)}(\mu)}=\frac{1}{\alpha_s^{(5)}(m_t)}+\frac{\beta_0^{(6)}}{\pi}\ln\frac{\mu^2}{m_t^2}, \tag{3.2}$$

$$\overline{m}_t^{(6)}(\mu)=m_t\left[1-\frac{\alpha_s^{(6)}(m_t)}{\pi}C_F\right]\left[\frac{\alpha_s^{(6)}(\mu)}{\alpha_s^{(6)}(m_t)}\right]^{\gamma_0/\beta_0^{(6)}}, \tag{3.3}$$

$$\overline{m}_b^{(6)}(\mu)=m_b\left[1-\frac{\alpha_s^{(5)}(m_b)}{\pi}C_F\right] \times\left[\frac{\alpha_s^{(5)}(m_t)}{\alpha_s^{(5)}(m_b)}\right]^{\gamma_0/\beta_0^{(5)}}\left[\frac{\alpha_s^{(6)}(\mu)}{\alpha_s^{(6)}(m_t)}\right]^{\gamma_0/\beta_0^{(6)}}, \tag{3.4}$$

where

$$\beta_0^{(n_f)}=\frac{1}{4}\left(\frac{11}{3}C_A-\frac{4}{3}T_F n_f\right),\quad \gamma_0=\frac{3}{4}C_F, \tag{3.5}$$

with $C_A=N_c$ and $T_F=1/2$, are the first coefficients of the Callan-Symanzik beta function and the quark-mass anomalous dimension, respectively. For simplicity, we use a common renormalization scale μ in $\alpha_s^{(6)}(\mu)$ and $\overline{m}_q^{(6)}(\mu)$. We study the cases $\sqrt{s}=500$ GeV and 800 GeV. As for the MSSM input parametrs, we consider the ranges $1<\tan\beta<40\approx m_t/m_b$ and $250<m_H<320$ GeV if $\sqrt{s}=500$ GeV or $400<m_H<620$ GeV if $\sqrt{s}=800$ GeV.

We now discuss the influence of the QCD corrections on the total cross sections of $e^+e^-\to t\bar{b}H^-$ and its charge conjugate counterpart, which we add. We start by selecting the renormalization scheme and scale that are most appropriate for the problem under consideration. For this purpose, we study the μ dependence of the Born and QCD-corrected results in two different renormalization schemes. The first one uses the pole masses m_t and m_b as basic parameters (OS scheme), while the second one uses m_t and the $\overline{\mathrm{MS}}$ mass $\overline{m}_b^{(6)}(\mu)$ as basic parametrs (mixed scheme). Both schemes employ the $\overline{\mathrm{MS}}$ definition of $\alpha_s^{(6)}(\mu)$. We refrain from utilizing $\overline{m}_t^{(6)}(\mu)$, which, in general, significantly deviates from

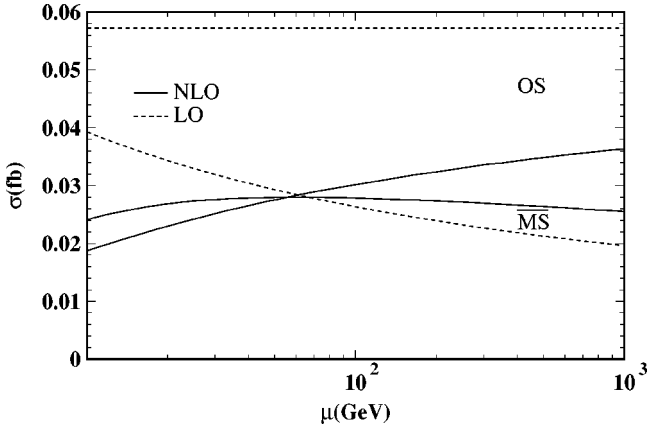

FIG. 4. Total cross section of $e^+e^- \to t\bar{b}H^-, \bar{t}bH^+$ as a function of μ for $\sqrt{s}=500$ GeV, $\tan\beta=40$, and $m_H=260$ GeV. The dashed and solid curves correspond to the Born and QCD-corrected results, respectively. The upper and lower sets of curves refer to the OS and mixed schemes, respectively.

m_t, as may be seen from Eq. (3.3). For, if we were to include the weak decays of the t and $\bar{t}$ quarks in our analysis, then, during the propagation of these quarks between their production and decay vertices, configurations near their *physical* mass shells would be kinematically favored. As a matter of fact, the experimentally measured invariant masses of their decay products are very close to m_t. In turn, the phase space of $e^+e^- \to t\bar{b}H^-$ would undergo a significant, yet artificial change of size if it were parametrized in terms of $\overline{m}_t^{(6)}(\mu)$ rather than m_t. On the other hand, the use of $\overline{m}_b^{(6)}(\mu)$ is predicated on the grounds that it automatically resums large logarithmic corrections that arise if the $t\bar{b}H^-$ Yukawa coupling is expressed in terms of m_b. A similar feature is familiar from the $H \to b\bar{b}$ decay in the SM [23]. This effect is particularly pronounced for large values of $\tan\beta$ because the $t\bar{b}H^-$ Yukawa coupling is then approximately proportional to the b-quark mass.

As a typical example, we consider in Fig. 4 the case of $\sqrt{s}=500$ GeV, $\tan\beta=40$, and $m_H=260$ GeV. We allow μ to vary over two orders of magnitude, from 10 to 1000 GeV. In the OS scheme, the Born result is μ independent, while the QCD-corrected one depends on μ via $\alpha_s^{(6)}(\mu)$. In the mixed scheme, the μ dependence enters at LO via $\overline{m}_b^{(6)}(\mu)$ and at NLO via $\alpha_s^{(6)}(\mu)$ and $\overline{m}_b^{(6)}(\mu)$. Obviously, the theoretical uncertainties due to scheme and typical scale variations are significantly reduced as we pass from LO to NLO. On the one hand, the OS-scheme to mixed-scheme ratio is brought down to the vicinity of unity, from 1.46–2.92 to 0.78–1.43, depending on the value of μ. On the other hand, the μ dependence within the mixed scheme is reduced by a factor of 5, from 0.020 fb to 0.004 fb in absolute terms. Furthermore, we observe that, in the OS scheme, the QCD corrections lead to a dramatic reduction of the cross section, by 36–67 %. As explained above, this is because they contain large logarithmic terms of the form $\alpha_s^{(6)}(\mu)\ln(M^2/m_b^2)$, where M is a generic mass scale in the ball park of some suitable average of the final-state-particle masses, m_b, m_t, and m_H. In the mixed scheme with μ of order M, such terms are shifted from the QCD corrections to the Born result, where they are absorbed into the running of $\overline{m}_b^{(6)}(\mu)$ from $\mu=m_b$ to $\mu=M$. This is reflected in Fig. 4 by the fact that, in the mixed scheme, the QCD corrections are relatively modest, ranging from -39% to $+30\%$. Unless otherwise stated, we shall henceforth work in the mixed scheme, which, for plausible values of μ, is superior to the OS scheme as far as the convergence properties are concerned.

Let us now turn to the question of how to fix the value of μ in a reasonable way. Scale-setting procedures frequently discussed in the literature include the concept of fastest apparent convergence (FAC) [24], the principle of minimal sensitivity (PMS) [25], and the proposal by Brodsky, Lepage, and Mackenzie (BLM) [26] to resum the leading light-quark contribution to the renormalization of the strong-coupling constant. The latter is not yet applicable to the problem under consideration, which is of LO in the strong-coupling constant. The FAC and PMS prescriptions lead us to select the values of μ where the Born and QCD-corrected results intersect and where the latter exhibits a local extremum, respectively. We observe from Fig. 4 that these two μ values approximately coincide, at about 60 GeV. Incidentally, in the close vicinity of these two μ values, also the QCD-corrected results in the OS and mixed schemes cross over, so that also the scheme dependence at NLO vanishes in this neighborhood, at least as for the two schemes considered here. Since the μ dependence is logarithmic, a democratic way of combining the three scales m_b, m_t, and m_H is by taking their geometric means, $\mu=\sqrt[3]{m_b m_t m_H}$. In the present case, this educated guess yields $\mu\approx 60$ GeV, which nicely agrees with the triply distinguished point identified above. We checked that this choice works similarly well for the case of $\sqrt{s}=800$ GeV, $\tan\beta=40$, and $m_H=410$ GeV. We shall henceforth employ it, with the understanding that Fig. 4 provides us with a useful estimate of the theoretical uncertainties due to scheme and typical scale variations, both at LO and NLO.

Figures 5 and 6 refer to $\sqrt{s}=500$ GeV, while Figs. 7 and 8 refer to $\sqrt{s}=800$ GeV. We investigate the m_H dependence for various values of $\tan\beta$ in Figs. 5 and 7 and the $\tan\beta$ dependence for typical values of m_H in Figs. 6 and 8. In each figure, we present the Born and QCD-corrected results in the mixed scheme with $\mu=\sqrt[3]{m_b m_t m_H}$. For comparison, in Figs. 6 and 8, we also present the corresponding results in the OS scheme with the same scale choice. We observe that the total cross sections exhibit minima close to $\tan\beta\approx\sqrt{m_t/m_b}\approx 6$, independently of order and scheme. This may be understood by observing that the average strength of the $t\bar{b}H^-$ Yukawa coupling, which is proportional to $\sqrt{m_t^2\cot^2\beta+m_b^2\tan^2\beta}$, is then minimal [27]. Depending on $\sqrt{s}$, $\tan\beta$, and m_H, the QCD corrections may be of either sign. By construction, they are generally rather modest in the mixed scheme, although they may reach a magnitude of 50% for specific values of $\sqrt{s}$, $\tan\beta$, and m_H, as may be seen from Fig. 7. On the other hand, in the OS scheme, the QCD corrections lead to a substantial reduction in cross section at large values of $\tan\beta$, by up to 50%. As explained above, this may be attributed to large logarithms arising from the $t\bar{b}H^-$ Yukawa coupling. Finally, we notice that Figs. 6 and 8 support the observations

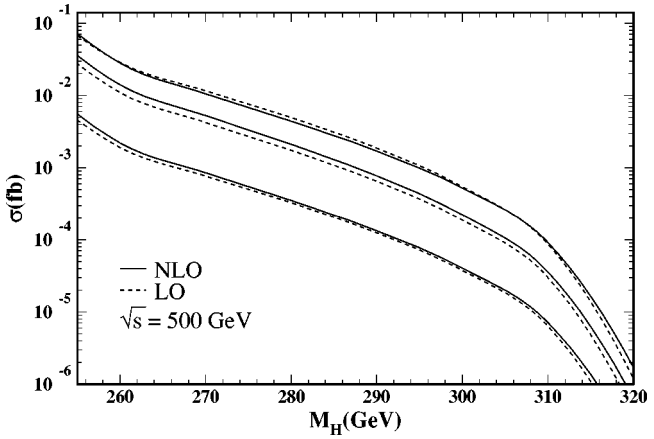

FIG. 5. Total cross section of $e^+e^- \to t\bar{b}H^-, \bar{t}bH^+$ without (dotted curves) and with (solid curves) QCD corrections in the mixed scheme as a function of m_H for $\sqrt{s}=500$ GeV and various values of $\tan\beta$. The middle, lower, and upper sets of curves correspond to $\tan\beta=2$, 6, and 40, respectively.

made in connection with Fig. 4. In fact, owing to our judicious scale choice, the Born and QCD-corrected results in the mixed scheme and the QCD-corrected result in the OS scheme all approximately coincide, which nicely demonstrates the perturbative stability in the mixed scheme and the feeble scheme dependence at NLO. By contrast, the perturbative stability in the OS scheme is rather poor at large values of $\tan\beta$.

It is interesting to investigate the relative importance of the contributions due to photon and Z-boson exchanges. To this end, we evaluate the photon-induced part of the total cross section by putting $\mathcal{V}_e=\mathcal{A}_e=0$ and compare it with the full result. We find that the bulk of the total cross section is due to photon exchange. In fact, for the typical values $\sqrt{s}=500$ GeV and $m_H=260$ GeV, the photon-induced part exhausts 78%, 80%, and 82% of the full result if $\tan\beta=2$, 6, and 40, respectively.

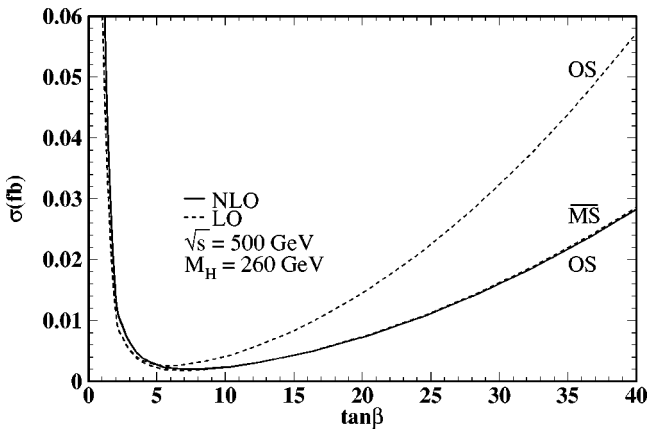

FIG. 6. Total cross section of $e^+e^- \to t\bar{b}H^-, \bar{t}bH^+$ without (dotted curves) and with (solid curves) QCD corrections as a function of $\tan\beta$ for $\sqrt{s}=500$ GeV and $m_H=260$ GeV. The upper and lower dotted curves refer to the OS and mixed schemes, respectively. The two solid curves referring to the OS and mixed schemes lie on top of each other.

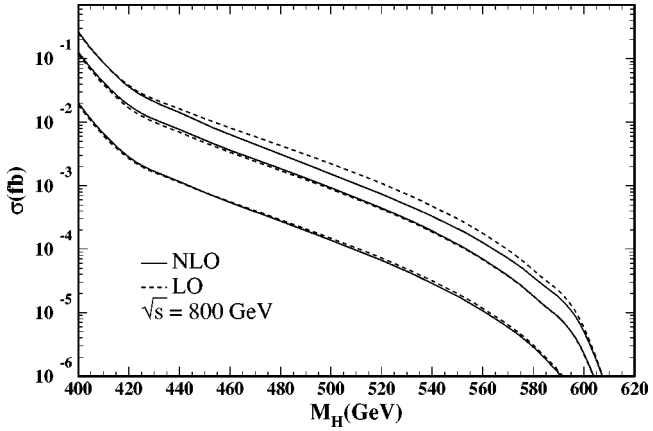

FIG. 7. Same as in Fig. 5, for $\sqrt{s}=800$ GeV.

IV. SUMMARY

We considered the process $e^+e^- \to t\bar{b}H^-$ and its charge-conjugate counterpart in the MSSM, which are among the dominant charged-Higgs-boson production mechanisms at a future e^+e^- LC if $m_t+m_b<\sqrt{s}/2<m_H<\sqrt{s}-m_t-m_b$, so that $t\to bH^+$ and $e^+e^- \to H^+H^-$ are not allowed kinematically. For $\sqrt{s}=500$ GeV and 800 GeV, this corresponds to the m_H windows $250\lesssim m_H\lesssim 320$ GeV and $400\lesssim m_H \lesssim 620$ GeV, respectively. We presented a compact Born formula for the cross sections of these processes and evaluated their dominant radiative corrections, which arise from QCD.

We regularized the IR singularities by introducing an infinitesimal gluon mass m_g and the UV ones by using dimensional regularization. The IR singularities cancelled when the virtual and soft real QCD corrections were combined and the UV ones upon renormalizing the masses and wave functions of the quarks in the Born transition-matrix element. We established these cancellations analytically. We separated the soft-gluon and hard-gluon contributions by introducing an unphysical gluon-energy cutoff $E_{\rm cut}$ and verified that their sum is insensitive to the choice of $E_{\rm cut}$ as long as $m_g \ll E_{\rm cut} \ll E_{\rm max}$ is satisfied.

We worked in a mixed renormalization scheme, where the strong-coupling constant and the b-quark mass are defined in

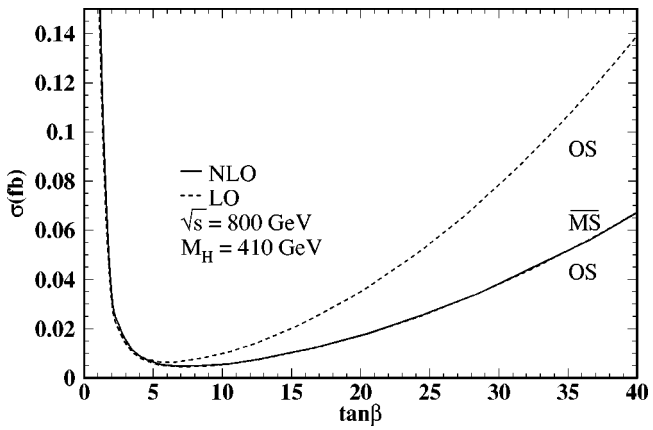

FIG. 8. Same as in Fig. 6, for $\sqrt{s}=800$ GeV and $m_H=410$ GeV.

the $\overline{\rm MS}$ scheme, while the t-quark mass is defined in the OS scheme. In this way, large logarithmic corrections that arise if the $t\bar{b}H^-$ Yukawa coupling is expressed in terms of the b-quark pole mass are automatically resummed, so that the convergence behavior of the perturbative expansion is improved. On the other hand, the use of the t-quark $\overline{\rm MS}$ mass does not entail such an improvement, but it rather appears somewhat unnatural from the physical point of view. The inclusion of the QCD corrections significantly reduces the theoretical uncertainties due to scheme and typical scale variations. We found that the QCD corrections to the total cross section may be of either sign, depending on the values of $\sqrt{s}$, $\tan\beta$, and m_H, and that they may reach a magnitude of up to 50%.

The e^+e^- TeV Energy Superconducting Linear Accelerator (TESLA), which is being developed and planned at DESY, has a design luminosity of $3.4\times10^{34}\,\mathrm{cm}^{-2}\mathrm{s}^{-1}$ ($5.8\times10^{34}\,\mathrm{cm}^{-2}\mathrm{s}^{-1}$) at $\sqrt{s}=500$ GeV (800 GeV), which corresponds to 340 fb^{-1}(580 fb^{-1}) per year [28]. Thus, a total cross section of typically 0.03 fb (0.07 fb) will yield about 10 (40) signal events per year.

As a by-product of our analysis, we confirmed the numerical results for the QCD-corrected total cross section of the SM process $e^+e^-\to q\bar{q}H$ obtained in Refs. [7,8].

ACKNOWLEDGMENTS

We thank Stefan Dittmaier for providing us with numerical results from Ref. [7], Thomas Hahn for helpful communications concerning FORMCALC [13], and Tao Han for a beneficial discussion preceding our work. F.M. thanks Stefan Berge for technical assistance regarding LOOPTOOLS [13]. B.A.K. is grateful to the CERN Theoretical Physics Division for its hospitality during a visit when this paper was finalized. This work was supported in part by the Deutsche Forschungsgemeinschaft through Grant No. KN 365/1-1, by the Bundesministerium für Bildung und Forschung through Grant No. 05 HT1GUA/4, and by Sun Microsystems through Academic Equipment Grant No. EDUD-7832-000332-GER.

APPENDIX A: BORN FORM FACTORS

In this appendix, we list compact expressions for the form factors $f_{\gamma\gamma}(x_1,x_2)$, $f_{\gamma Z}(x_1,x_2)$, and $f_{ZZ}(x_1,x_2)$ appearing in Eq. (2.7). It is possible to combine the propagators of the t quark, b quark, and H^- boson with their couplings to the photon and Z boson by defining the effective couplings

$$\mathcal{Q}_q=-\frac{2c_w s_w Q_q}{1-x_q},\qquad \mathcal{V}_q=\frac{I_q-2s_w^2Q_q}{1-x_q},$$

$$\mathcal{A}_q=\frac{I_q}{1-x_q},\quad \mathcal{H}_\gamma=\frac{2c_w s_w}{1-x_3},\quad \mathcal{H}_Z=\frac{s_w^2-c_w^2}{1-x_3},\tag{A1}$$

where $q=t,b$ and we have identified $x_t=x_1$ and $x_b=x_2$. The $t\bar{b}H^-$ Yukawa coupling introduces $\tan\beta$ dependence through the combinations

$$T_\pm=a_1\cot^2\beta\pm a_2\tan^2\beta.\tag{A2}$$

We find

$$\begin{aligned}
f_{ZZ}=&\,2\mathcal{V}_t^2\{4a_1a_2(2+2a_1-x_1)+T_+[(1+2a_1)(1+a_1+a_2-a_3-x_1)-x_2(1-x_1)]\}+4\mathcal{V}_t\mathcal{V}_b\{2a_1a_2(4+2a_1+2a_2-2a_3\\
&-x_1-x_2)+T_+[(1+a_2-a_3-x_1)(1+a_1-a_3-x_2)+(a_1+a_2)(1+a_1+a_2-a_3)-a_1a_2]\}+2\mathcal{V}_b^2\{4a_1a_2(2+2a_2-x_2)\\
&+T_+[(1+2a_2)(1+a_1+a_2-a_3-x_2)-x_1(1-x_2)]\}-4\mathcal{V}_t\mathcal{A}_tT_-[(1-x_2)(1+2a_1-x_1)-a_1+a_2-a_3]\\
&+4\mathcal{V}_t\mathcal{A}_bT_-[(1+a_2-a_3-x_1)(1+a_1+2a_2-a_3-x_2)+(a_1-a_2)(1+a_1+a_2-a_3)-3a_1a_2]-4\mathcal{V}_b\mathcal{A}_tT_-[(1+a_1-a_3\\
&-x_2)(1+2a_1+a_2-a_3-x_1)-(a_1-a_2)(1+a_1+a_2-a_3)-3a_1a_2]+4\mathcal{V}_b\mathcal{A}_bT_-[(1-x_1)(1+2a_2-x_2)+a_1-a_2-a_3]\\
&-2\mathcal{A}_t^2\{4a_1a_2(2+6a_1-3x_1)-T_+[(1-6a_1)(1+a_1+a_2-a_3-x_1)-x_2(1-x_1)]\}-4\mathcal{A}_t\mathcal{A}_b\{2a_1a_2(4+6a_1+6a_2\\
&-6a_3-3x_1-3x_2)+T_+[(1+2a_1+a_2-a_3-x_1)(1+a_1+2a_2-a_3-x_2)-(a_1+a_2)(1+a_1+a_2-a_3)\\
&+7a_1a_2]\}-2\mathcal{A}_b^2\{4a_1a_2(2+6a_2-3x_2)-T_+[(1-6a_2)(1+a_1+a_2-a_3-x_2)-x_1(1-x_2)]\}+2\mathcal{V}_t\mathcal{H}_Z\{4a_1a_2(1-2a_1\\
&+2a_2-2a_3-x_2)+T_+[(1+2a_2-2a_3-x_1)(1-a_1-a_2-a_3-x_1-x_2)-2a_1(a_1+a_3)+2a_2(1+a_1\\
&+2a_2-2a_3)]\}-2\mathcal{V}_b\mathcal{H}_Z\{4a_1a_2(1+2a_1-2a_2-2a_3-x_1)+T_+[(1+2a_1-2a_3-x_2)(1-a_1-a_2-a_3-x_1-x_2)\\
&-2a_2(a_2+a_3)+2a_1(1+2a_1+a_2-2a_3)]\}-2\mathcal{A}_t\mathcal{H}_ZT_-[(1+2a_1+2a_2-2a_3-x_1)(1+a_1-a_2-a_3-x_1-x_2)\\
&+2a_2(1-2a_1+2a_2-2a_3)]-2\mathcal{A}_b\mathcal{H}_ZT_-[(1+2a_1+2a_2-2a_3-x_2)(1-a_1+a_2-a_3-x_1-x_2)+2a_1(1+2a_1-2a_2\\
&-2a_3)]-\mathcal{H}_Z^2[4a_1a_2(3-4a_3-2x_1-2x_2)+T_+(3-4a_3-2x_1-2x_2)(1+a_1+a_2-a_3-x_1-x_2)].
\end{aligned}\tag{A3}$$

The formulas for $f_{\gamma\gamma}(x_1,x_2)$ and $f_{\gamma Z}(x_1,x_2)$ may be obtained from Eq. (A3) by adjusting the coupling constants. Specifically, one has to substitute

$$\mathcal{V}_q \to \mathcal{Q}_q, \quad \mathcal{A}_q \to 0, \quad \mathcal{H}_Z \to \mathcal{H}_\gamma \tag{A4}$$

in the first case and

$$\begin{aligned} &\mathcal{V}_q\mathcal{V}_{q'} \to \mathcal{Q}_q\mathcal{V}_{q'} + \mathcal{Q}_{q'}\mathcal{V}_q, \quad \mathcal{V}_q\mathcal{A}_{q'} \to \mathcal{Q}_q\mathcal{A}_{q'}, \\ &\mathcal{A}_q\mathcal{A}_{q'} \to 0, \quad \mathcal{V}_q\mathcal{H}_Z \to \mathcal{Q}_q\mathcal{H}_Z + \mathcal{V}_q\mathcal{H}_\gamma, \\ &\mathcal{A}_q\mathcal{H}_Z \to \mathcal{A}_q\mathcal{H}_\gamma, \quad \mathcal{H}_Z^2 \to 2\mathcal{H}_\gamma\mathcal{H}_Z \end{aligned} \tag{A5}$$

in the second one $(q,q'=t,b)$.

APPENDIX B: FOUR-PARTICLE PHASE SPACE

In this appendix, we present the parametrization of the four-particle phase space that we use to evaluate the hard-gluon contribution. We generically denote the four-momenta and masses of the final-state particles as p_i and m_i $(i=1,\ldots,4)$, respectively. Similarly as in Sec. II A, we define $p=\sum_{i=1}^4 p_i$, $s=p^2$, $a_i=m_i^2/s$, $x_i=2p\cdot p_i/s$, and $y_i=\sqrt{x_i^2-4a_i}$. Due to four-momentum conservation, we have $\sum_{i=1}^4 x_i=2$. We decompose the four-particle phase space into three nested two-particle phase spaces as [29]

$$\begin{aligned} d\mathrm{PS}_4(p;p_1,p_2,p_3,p_4) = {} & \frac{ds_{12}ds_{34}}{(2\pi)^2} d\mathrm{PS}_2(p;p_{12},p_{34}) \\ & \times d\mathrm{PS}_2(p_{12};p_1,p_2) \\ & \times d\mathrm{PS}_2(p_{34};p_3,p_4), \end{aligned} \tag{B1}$$

where $p_{ij}=p_i+p_j$ and $s_{ij}=p_{ij}^2$, with $(i,j)=(1,2),(3,4)$. As in Sec. II A, we work in the c.m. frame, take the z axis of the coordinate system to point along $\boldsymbol{k}_1=-\boldsymbol{k}_2$, and choose the x axis arbitrarily. We have $\boldsymbol{p}_{12}=-\boldsymbol{p}_{34}$ and $|\boldsymbol{p}_{12}|=(1/2)\sqrt{\lambda(s,s_{12},s_{34})}/s$. Using

$$d\mathrm{PS}_2(p;p_{12},p_{34}) = \frac{|\boldsymbol{p}_{12}|}{(4\pi)^2\sqrt{s}} d\cos\theta_{12} d\phi_{12},$$

$$d\mathrm{PS}_2(p_{ij};p_i,p_j) = \frac{1}{(4\pi)^2|\boldsymbol{p}_{ij}|} dp_i^0\, d\phi_i, \tag{B2}$$

where θ_{12} and ϕ_{12} are the polar and azimuthal angles of $\boldsymbol{p}_{12}$, respectively, and ϕ_i is the azimuthal angle of $\boldsymbol{p_i}$ with respect to the axis pointing along $\boldsymbol{p_{ij}}$ measured from the plane spanned by $\boldsymbol{k}_1$ and $\boldsymbol{p_{ij}}$, we obtain

$$\begin{aligned} d\mathrm{PS}_4(p;p_1,p_2,p_3,p_4) = {} & \frac{8}{(4\pi)^8\sqrt{\lambda(s,s_{12},s_{34})}} \\ & \times ds_{12}\, ds_{34}\, d\cos\theta_{12}\, d\phi_{12} \\ & \times dp_1^0\, d\phi_1\, dp_3^0\, d\phi_3. \end{aligned} \tag{B3}$$

Owing to the azimuthal symmetry of the problem under consideration, the integration over ϕ_{12} is trivial, and we may choose $\boldsymbol{p}_{12}$ to lie in the x-z plane. If we now rotate the coordinate system in such a way that $\boldsymbol{p}_{12}$ points along the z axis and $\boldsymbol{p}_1$ lies in the x-z plane, then $\theta=\theta_{12}$ and $\phi=\pi-\phi_1$ define the direction of $\boldsymbol{k}_1$. Introducing $z_{ij}=s_{ij}/s$, we thus have

$$\begin{aligned} d\mathrm{PS}_4(p;p_1,p_2,p_3,p_4) = {} & \frac{s^2}{(4\pi)^7\sqrt{\lambda(1,z_{12},z_{34})}} \\ & \times dz_{12}\, dz_{34} dx_1 dx_3 d\phi_3 \\ & \times d\cos\theta\, d\phi. \end{aligned} \tag{B4}$$

As explained in Eq. (2.6), the integrations over $\cos\theta$ and ϕ can be exploited to transform the leptonic tensor $L^{\mu\nu}$ defined by Eq. (2.5), which depends on k_1 and k_2, into one depending only on p, so as to preclude scalar products of the type $k_i\cdot p_j$. The residual scalar products read

$$\begin{aligned} p_1\cdot p_2 &= \frac{s}{2}(z_{12}-a_1-a_2), \\ p_3\cdot p_4 &= \frac{s}{2}(z_{34}-a_3-a_4), \\ p_1\cdot p_3 &= \frac{s}{4}[x_1x_3-y_1y_3(\sin\theta_1\sin\theta_3\cos\phi_3 \\ &\qquad -\cos\theta_1\cos\theta_3)], \\ p_1\cdot p_4 &= \frac{s}{2}(x_1-z_{12}-a_1+a_2)-p_1\cdot p_3, \\ p_2\cdot p_3 &= \frac{s}{2}(x_3-z_{34}-a_3+a_4)-p_1\cdot p_3, \\ p_2\cdot p_4 &= \frac{s}{2}(1-x_1-x_3+a_1-a_2+a_3-a_4)+p_1\cdot p_3, \end{aligned} \tag{B5}$$

where θ_i is the angle enclosed between $\boldsymbol{p_{ij}}$ and $\boldsymbol{p_i}$. It is determined by

$$\cos\theta_i = \frac{x_i(1+z_{ij}-z_{kl})-2(z_{ij}+a_i-a_j)}{y_i\sqrt{\lambda(1,z_{ij},z_{kl})}}, \tag{B6}$$

with $(i,j),(k,l)=(1,2),(3,4)$ and $(i,j)\neq(k,l)$. Furthermore, we have

$$x_j = 1-x_i+z_{ij}-z_{kl}. \tag{B7}$$

The limits of integration are

$$(\sqrt{a_1}+\sqrt{a_2})^2<z_{12}<(1-\sqrt{a_3}-\sqrt{a_4})^2,$$

$$(\sqrt{a_3}+\sqrt{a_4})^2<z_{34}<(1-\sqrt{z_{12}})^2,$$

$$x_i^-<x_i<x_i^+,$$

$$0<\phi_3<2\pi, \tag{B8}$$

where

$$x_i^{\pm}=\frac{1}{2z_{ij}}[(1+z_{ij}-z_{kl})(z_{ij}+a_i-a_j) \pm \sqrt{\lambda(1,z_{ij},z_{kl})\lambda(z_{ij},a_i,a_j)}]. \tag{B9}$$

For the application in Sec. II C, it is convenient to assign the indices 1, 2, 3, and 4 to the t quark, $\bar{b}$ quark, gluon, and H^- boson, respectively. Then, the hard-gluon condition $q^0>E_{\rm cut}$ may be implemented by substituting $x_3^- \to \max(x_3^-, 2E_{\rm cut}/\sqrt{s})$ in Eq. (B8). Furthermore, we have $a_3=0$ throughout this appendix.

[1] S. Komamiya, Phys. Rev. D **38**, 2158 (1988).
[2] S. Kanemura, S. Moretti, and K. Odagiri, J. High Energy Phys. **02**, 011 (2001).
[3] S. Kanemura, Eur. Phys. J. C **17**, 473 (2000); A. Arhrib, M. Capdequi Peyranere, W. Hollik, and G. Moultaka, Nucl. Phys. **B581**, 34 (2000).
[4] H.E. Logan and S. Su, Phys. Rev. D **66**, 035001 (2002); Report No. CALT-68-2392, FERMILAB-Pub-02/110-T, and hep-ph/0206135.
[5] S. Moretti, Report No. CERN-TH/2002-137, IPPP/02/30, DCPT/02/60, and hep-ph/0206208.
[6] A. Djouadi, J. Kalinowski, and P.M. Zerwas, Z. Phys. C **54**, 255 (1992).
[7] S. Dittmaier, M. Krämer, Y. Liao, M. Spira, and P.M. Zerwas, Phys. Lett. B **441**, 383 (1998).
[8] S. Dawson and L. Reina, Phys. Rev. D **59**, 054012 (1999).
[9] S. Dawson and L. Reina, Phys. Rev. D **60**, 015003 (1999); S. Dittmaier, M. Krämer, Y. Liao, M. Spira, and P.M. Zerwas, Phys. Lett. B **478**, 247 (2000).
[10] G.P. Lepage, J. Comput. Phys. **27**, 192 (1978).
[11] W.A. Bardeen, A.J. Buras, D.W. Duke, and T. Muta, Phys. Rev. D **18**, 3998 (1978).
[12] J. Küblbeck, M. Böhm, and A. Denner, Comput. Phys. Commun. **60**, 165 (1990); T. Hahn, *ibid.* **140**, 418 (2001); T. Hahn and C. Schappacher, *ibid.* **143**, 54 (2002).
[13] T. Hahn and M. Perez-Victoria, Comput. Phys. Commun. **118**, 153 (1999); T. Hahn, Acta Phys. Pol. B **30**, 3469 (1999); Nucl. Phys. B (Proc. Suppl.) **89**, 231 (2000).
[14] J.A.M. Vermaseren, *Symbolic Manipulation with FORM* (Computer Algebra Netherlands, Amsterdam, 1991).
[15] W. Beenakker and A. Denner, Nucl. Phys. **B338**, 349 (1990).
[16] G. 't Hooft and M. Veltman, Nucl. Phys. **B153**, 365 (1979); A. Denner, Fortschr. Phys. **41**, 307 (1993).
[17] A.H. Hoang, M. Jezabek, J.H. Kühn, and T. Teubner, Phys. Lett. B **338**, 330 (1994).
[18] S.D. Ellis, R. Kleiss, and W.J. Stirling, RA(NDOM) M(OMENTA) B(EAUTIFULLY) O(RGANIZED) (unpublished).
[19] T. Kinoshita, J. Math. Phys. **3**, 650 (1962); T.D. Lee and M. Nauenberg, Phys. Rev. **133**, B1549 (1964).
[20] Particle Data Group, D.E. Groom *et al.*, Eur. Phys. J. C **15**, 1 (2000).
[21] B.A. Kniehl, G. Kramer, and B. Pötter, Phys. Rev. Lett. **85**, 5288 (2000).
[22] B.A. Kniehl, Z. Phys. C **72**, 437 (1996).
[23] E. Braaten and J.P. Leveille, Phys. Rev. D **22**, 715 (1980).
[24] G. Grunberg, Phys. Lett. **95B**, 70 (1980); **110B**, 501(E) (1982); Phys. Rev. D **29**, 2315 (1984).
[25] P.M. Stevenson, Phys. Rev. D **23**, 2916 (1981); Phys. Lett. **100B**, 61 (1981); Nucl. Phys. **B203**, 472 (1982); Phys. Lett. **231**, 65 (1984).
[26] S.J. Brodsky, G.P. Lepage, and P.B. Mackenzie, Phys. Rev. D **28**, 228 (1983); S.J. Brodsky and H.J. Lu, *ibid.* **51**, 3652 (1995).
[27] A. Krause, T. Plehn, M. Spira, and P.M. Zerwas, Nucl. Phys. **B519**, 85 (1998).
[28] J. Andruszkow *et al.*, TESLA Technical Design Report, Part II, edited by R. Brinkmann, K. Flöttmann, J. Rossbach, P. Schmüser, N. Walker, and H. Weise, Report No. DESY 2001-011, ECFA 2001-209, TESLA Report 2001-23, and TESLA-FEL 2001-05, 2001.
[29] E. Byckling and K. Kajantie, *Particle Kinematics* (Wiley, London, 1973).